Nova Scientia
Revista de Investigación de la Universidad De La Salle Bajío

Nº 27, Vol. 13 (3), 2021. ISSN 2007 – 0705, pp.: 1 – 25
doi.org/10.21640/ns.v13i27.2877

Caracterización y estudio termoluminiscente de ZnO sin dopar y ZnO dopado con Tb sintetizados por el método de rocío pirolítico
Characterization and thermoluminescence study of gamma irradiated Tb-doped ZnO and undoped ZnO synthesized by spray pyrolysis method

A. Ortiz-Morales [1, 2] 0000-0002-6897-0789
M. García-Hipólito [3]
E. Cruz-Zaragoza [2] 0000-0003-0422-7854
R. Gómez-Aguilar [1] 0000-0002-5945-5929

[1] Instituto Politécnico Nacional, UPIITA ✉ alortizm@ipn.mx
[2] Universidad Nacional Autónoma de México, Instituto de Ciencias Nucleares
[3] Universidad Nacional Autónoma de México, Instituto de Investigaciones en Materiales

Palabras clave: efectos de la radiación ionizante; termoluminiscencia; parámetros cinéticos; micro-material; microscopía electrónica de barrido; dispersión Raman; fotoluminiscencia; difracción de rayos X; deconvolución de curvas de brillo; detector de radiación
Keywords: ionizing radiation effects; thermoluminescence; kinetic parameters; micro-material; scanning electron microscopy; Raman dispersion; photoluminescence; X-ray diffraction; deconvolution glow curve; radiation detector
PACS: 61.80.-x; 78.60.Kn; 87.53.Bn; 61.82.Pv

Recepción: 24 – 24 – 2021 / Aceptación: 24 – 06 – 2021

Resumen

Se prepararon micro fósforos termoluminiscentes (TL) de ZnO no dopado y ZnO dopado con Tb usando el método de rocío pirolítico, mostrando alta resistencia a campos de radiación gamma. La microscopía electrónica de barrido exhibe varillas cristalinas con morfología hexagonal (0,1-0,4 µm de diámetro y aproximadamente 1 µm de longitud). El espectro de la dispersión Raman revela una forma de würtzita. El espectro fotoluminiscente (FL) de las películas de óxido de zinc irradiadas indica la generación de defectos producidos por la irradiación gamma, que resulta en un aumento de la probabilidad de recombinación del electrón hueco-excitón. El espectro fotoluminiscente muestra las bandas de emisión $5D_4$-$7F_j$ = 6,5,4,3 estas transiciones son atribuidas al dopante Tb^{3+} en este fósforo. Los patrones de difracción de rayos X para ambas películas (ZnO sin dopar y ZnO dopado con Tb) son típicos de la estructura cristalina de óxido de zinc, sin un efecto notable sobre los iones Tb. Las propiedades dosimétricas, para ambas muestras, muestran una señal de desvanecimiento termoluminiscente baja y una reproducibilidad de la intensidad termoluminiscente para ZnO sin dopar y ZnO dopado con Tb de 29 y 57%, respectivamente. Los parámetros cinéticos; energía de activación *E*, factor de frecuencia *s* y R_m, se obtuvieron mediante la Deconvolución Computarizada de la Curva de brillo (DCCB) asumiendo un modelo cinético de orden mixto (MCOM). Los resultados muestran que el MCOM describió bien las curvas de brillo de las películas de óxido de zinc. Los efectos

de la velocidad de calentamiento produjeron una ampliación del pico de brillo ubicado a 420 K. Para propósitos como detector de radiación, se obtuvo el número atómico efectivo (Z_{eff}): 27.74 y 56.47 para la muestra de ZnO sin dopar y ZnO dopado con Tb, respectivamente. Las muestras se expusieron a radiación gamma en un amplio intervalo de dosis de 0.25 a 20 kGy. Las propiedades TL de las muestras de ZnO sin dopar y de ZnO dopado con Tb muestran que estos materiales podrían usarse para detectar altas dosis en un campo de radiación gamma.

Abstract

High gamma dose-resistant undoped ZnO and Tb-doped ZnO thermoluminescent (TL) micro-phosphors were prepared by the spray pyrolysis method. Scanning electron microscopy shows crystalline rods with hexagonal morphology, (0.1-0.4 μm diameter, and about 1 μm length). Raman spectra dispersion reveals a würtzite form. Photoluminescence (PL) study of irradiated zinc oxide films indicates the generation of defects produced by gamma irradiation resulting in an increased probability of electron-hole exciton recombination. PL spectrum shows emission bands from $^5D_4$-$^7F_{j=6,5,4,3}$ transitions ascribed to Tb^{3+} dopant in zinc oxide phosphor. X-ray diffraction patterns for both types of films growth (undoped ZnO and Tb-doped ZnO) are typical of zinc oxide crystalline structure, with no noticeable effect of Tb ions. Dosimetric properties, for both samples, show a low TL fading signal and TL reproducibility signal for undoped ZnO and Tb-doped ZnO samples was 29 and 57 %, respectively. The kinetic parameters such as activation energy *E*, frequency factor *s*, and R_m values, were obtained by Computerized Glow Curve Deconvolution (CGCD) assuming Mixed Order Kinetic model (MOK). The results show that the MOK well described the glow curves of zinc oxide films. The heating rate effects produced a broadening of glow peak located at 420 K. For purposes like radiation detector, atomic effective number (Z_{eff}) was obtained: 27.74 and 56.47 for undoped ZnO and Tb-doped ZnO samples, respectively. The samples were exposed to gamma radiation in a wide range of 0.25–20 kGy dose. TL properties of undoped ZnO and Tb-doped ZnO samples show that these materials could be used to detect high doses in a gamma radiation field.

Introduction

Zinc oxide (ZnO) can be synthesized in micro-nanostructured particles with different shapes and sizes, having a wide 3.37 eV gap and a high exciton binding energy. This oxide generally exhibits emissions in the near ultraviolet (around 380 nm) and in visible region (blue and green-

yellow); emission at 380 nm is called near band edge (NBE) emission and is due to exciton recombination effect (Ahsanulhaq *et al.*, 2007; Umar *et al.*, 2006). It is a transparent semiconductor, attractive for potential novel applications in electronics, sensors, transducers, biomedical applications, and integrated circuit technology.

Several processes to obtain zinc oxide with different dopants ions can be found: a wet chemical route with calcination procedure was used to synthesize Y-doped and Tb-doped ZnO nanocrystals (Pal *et al*., 2006; Parta *et al*., 2013), also undoped and Al-doped ZnO thin films were prepared by the sol-gel process (Tiekun *et al*., 2009), and ZnO:Tb^{3+} nanotube arrays were obtained using Anodic Alumina Membranes (AAMs) via electro-deposition method (Shihua *et al*., 2010). Rare earth-doped ZnO materials have been attracting interest for possible applications in high power lasers, visible emitting phosphors in displays, and other optoelectronic devices.

The TL properties of undoped zinc oxide (Cruz-Vazquez *et al.*, 2005; Pal *et al.*, 2006) and doped with Ce, Yb, Tb, Eu, Dy, and La ions, have been analyzed by different authors (Kucuk *et al.*, 2016; Goswami *et al*., 2015; Sunta *et al*., 2002) Ce or Yb dopant ions introduced in zinc oxide, have a quenching effect on the TL emission but improve some TL responses such as fading and dose-response at low doses from 143 mGy up to 60 Gy from beta radiation. Is important to mention that zinc oxide is very sensible to rare-earth dopant ions and their glow curves intensity depends on different doping concentration, however, there are few reports on Tb-doped zinc oxide films using high doses of gamma radiation. The Yb dopant in ZnO improves stability of trapped charges at shallow/low temperature (Pal *et al*., 2006).

Also, zinc oxide semiconductor nanocrystals are important in the emerging field of blue/UV optoelectronics and nanotechnology. When Tb-doped ZnO is obtained through implantation ions, the characteristic green emission bands associated with Tb generated by $^5D_4 \rightarrow {}^7F_{j=5,4}$ transitions have strongly increased in their intensities after thermal annealing (Cetin *et al*., 2009). The doping of Tb^{3+} has been used to produce green phosphor emitting light at 543 nm and with a long decay time (Badalawa *et al*., 2006). Rare-earth doped zinc oxide phosphors are very attractive materials due to their optical emissions from the 4f-4f or 4f-5d transitions. However, their optical and luminescent properties strongly depend on the preparation route (Klingshirn *et al*., 2007; Daksh *et al., 2016)*.

Photoluminescence (PL) property of Ce-doped ZnO nanophosphor showed green and red emissions due to the charge transfer at oxygen vacancies and to the Ce ion transitions, respectively (Sudheesh *et al.*, 2014). Pal and Manam (Parta *et al*., 2013) prepared Tb-doped ZnO by co-precipitation method at room temperature, and its morphological structure is

composed of nanoflakes and nanorods. The glow curves peaked at 255 °C for the Tb-doped sample and at 190 °C for undoped ZnO. The terbium dopant improved the TL intensity of Tb-doped ZnO, and it was higher than that of the undoped zinc oxide sample. However, linear dose-response analysis and the X-ray doses were not specified. Recently, Isik (Isik, *et al*., 2019) obtained undoped ZnO in nanoparticle form via sol-gel synthesis.

The TL glow curves exhibited broad and asymmetrical glow curves with a maximum temperature of about 83 K, including three overlapped peaks at 55, 85, and 118 K. In that case, the undoped ZnO nanoparticles may be useful for low-temperature dosimetry but not for room temperature dosimetry. These characteristics suggest that TL properties of ZnO phosphor can be improved by using Tb as dopant in ZnO host lattice. In this work, undoped ZnO and Tb-doped ZnO films (micro and nanostructured) were synthesized, characterized, and irradiated between 0.25-20 kGy doses to study the feasibility of this material as a gamma TL detector for high radiation field.

Materials and methods

To synthesize the ZnO films, a solution precursor was prepared using zinc nitrate ($Zn(NO_3)_2.6H_2O$) as Zn and O sources and hexamethylenetetramine [$(CH_3)_6N_4$] as surfactant and catalyst under the hydrothermal reaction mechanism, in which the $[Zn(OH)_4]^{-2}$ radical plays an important role in the ZnO rods assisted-hydrothermal synthesis (Baruah *et al*., 2009). The powder synthesized by assisted-hydrothermal process (above mentioned) was dissolved in deionized water (1 gram in 500 ml). This mixture constituted the precursor source for synthesis of samples (ZnO and ZnO:Tb) using ultrasonic spray pyrolysis method. The experimental arrangement of this technique has been presented previously (Cetin *et al*., 2009). In this case, an aerosol is formed from the precursor solution, which is directed thought a carrier gas, towards a previously heated substrate. Solvents in solution vaporize when solution mist comes in contact with hot substrate causing a solid coating on the substrate. In this case, optimal doping with Tb was achieved by adding $TbCl_3{\cdot}6H_2O$ (1 at. %) in relation to the Zn content in this solution. The carrier gas flow (filtered air) was 12 l/min and solution flow rate was 4 ml/min. The substrate temperature during deposition was fixed at 400 ^oC; substrates used were aluminum foil discs.

Before irradiation, the samples were annealed at 770 K for 1 hour. After cooling down to room temperature (RT) zinc oxide samples were inserted in a black box to avoid any environmental light effect. The samples were exposed to gamma photons from ^{60}Co of Gammabeam 651PT Nordion irradiator, with 170 Gy/min dose rate. The TL measurements

were carried out using a Harshaw TLD reader model 3500. Nitrogen gas was allowed to flow into the reading chamber during the readout to eliminate any spurious TL signals. Constant heating rates of 2, 5, 10, 15, 20, and 40 K/s were used. Both types of equipment, the panoramic irradiator, and the TLD reader are placed at the Nuclear Science Institute-UNAM.

The morphology of the samples was analyzed using a JEOL JSM 840 A scanning electron microscopy (SEM), supplied by the Research Materials Institute-(IIM)-UNAM. The TL signal was integrated from room temperature (300 K) up to 700 K. Photoluminescence spectra were recorded on a NanoLog fluorometer from Horiba-Jobin-Yvon exciting from 220 to 1000 nm with a Xenon arc lamp supplied by the Solid State Laboratory of the Physics and Mathematics Superior School (ESFM-IPN). For Raman scattering spectroscopy a Perkin-Elmer Raman Station 400F, located at the Nanosciences-micro and Nanotechnologies Center-IPN was used (excitation source 350 Mw, near infrared 785 nm laser, 95-3500 cm^{-1} Raman shift , 4 cm^{-1} FWHM). The X-ray analysis was made using a Bruker AXS D8-Advance diffractometer (30 kV, 0.5 deg. min^{-1}, $5°<2\theta<80°$) with Cu-Kα radiation of 0.15418 nm wavelength supplied by the IIM-UNAM.

Results and discussion

Sample characterization

Scanning Electron Microscopy (SEM) of undoped ZnO shows micro-nanostructures (fig 1.a) with hexagonal crystalline shape and the preference of this material to grow in a well-formed rod structure. The surface morphology is formed by overlapping ZnO micro-nanorods. The diameter and length average values were about 0.1-0.4 and 1 μm, respectively. A random inspection over the substrate area showed that it was uniformly covered by this kind of microstructure. It is possible to observe uniformity in diameters and lengths of the hexagonal crystals.

These characteristics possibly result from typical growing processes of these films properly influenced by local chemical and/or thermodynamic environment. The nature of substrate also influences on film growth; this coating formation is a consequence of reactive nature of aluminum substrate, which is not the case for other substrates. Incorporation of Tb ions into ZnO host lattice produces some changes in the surface morphology of Tb-doped ZnO films (fig. 1b). In this case, it is possible to observe hexagonal rods with larger diameters mainly and lengths. An additional kind of microstructures was observed: some particles consisting of rods emerging radially from a single point. Similar results have been obtained in other studies on ZnO: Tb^{3+} (Sreeja *et al*., 2017).

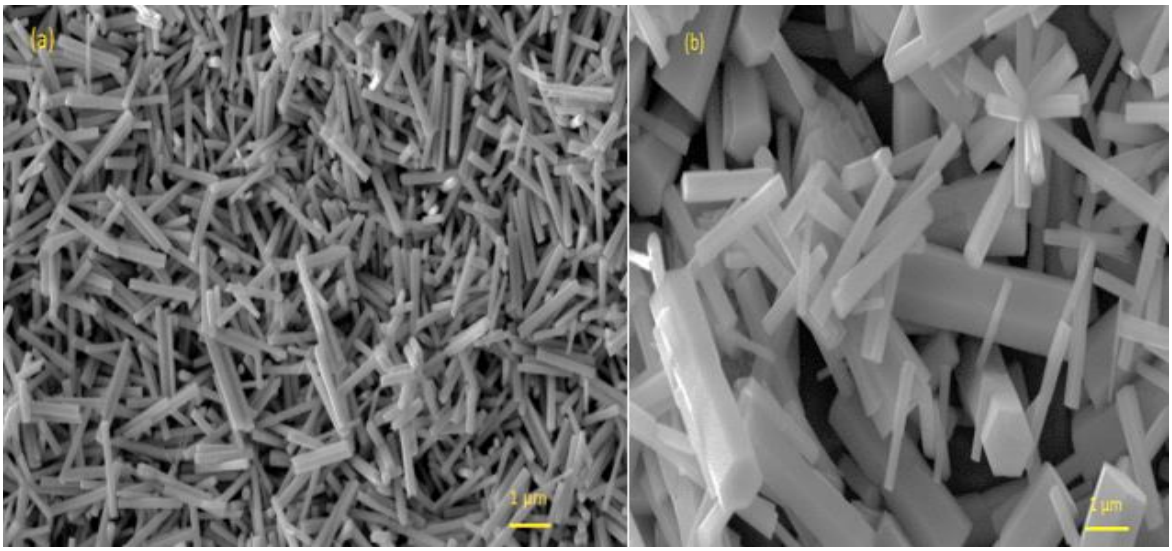

Fig. 1. Scanning Electron Microscopy micrographs of the surface morphology for; **a)** undoped ZnO, and **b)** Terbium-doped ZnO. The diameter (d) and length (l) average values are indicated.
Fig. 1. Micrografia de la morfología de la superficie, realizada con la técnica microscopia electronica de barrido para las muestras: **a)** ZnO no dopada, **b)** ZnO dopada con terbio. Los valores del diámetro (d) y la longitud(l) están indicadas.

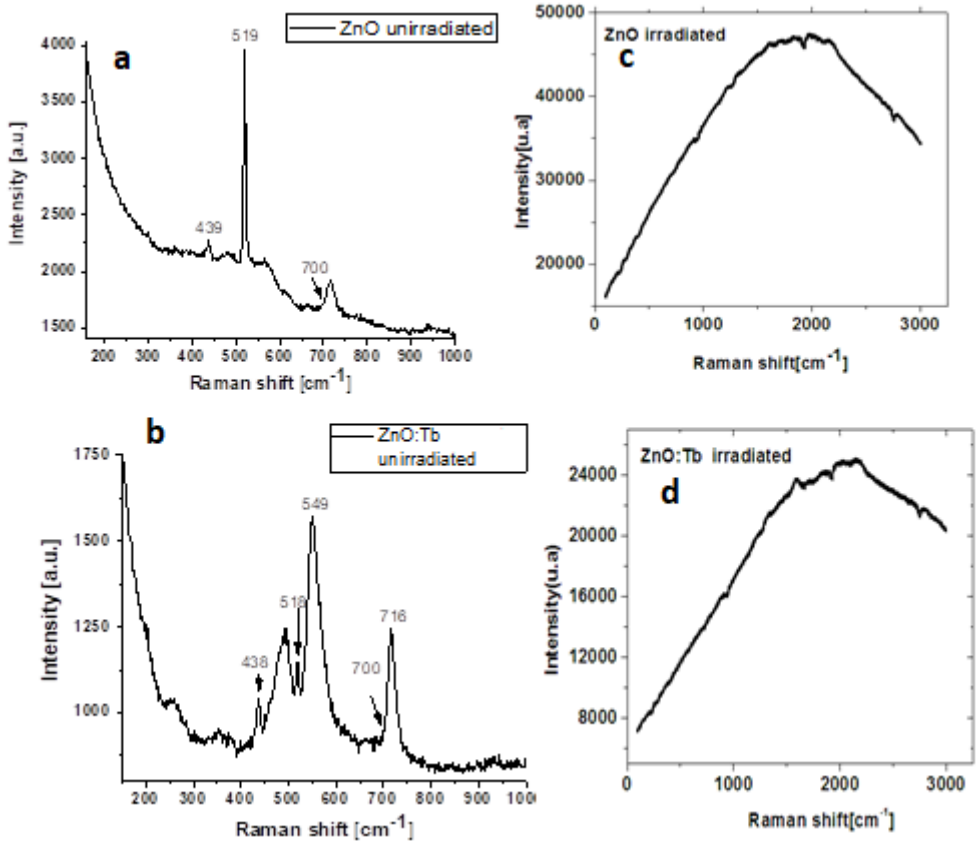

Fig. 2. a) and **b)** Raman spectra of the unirradiated samples, **c)** and **d)** corresponding to ZnO and ZnO:Tb gamma-irradiated samples, respectively.
Fig. 2. a) y **b)** Espectros Raman de las muestras no irradiadas, **c)** y **d)** corresponden a las muestras de ZnO y ZnO:Tb irradiadas con fotones gama, respectivamente.

Raman analysis of unirradiated ZnO samples exhibited bands peaked at 439, 519, and 716 cm^{-1} (fig 2.a). These bands are ascribed to the zinc oxide, and the one located at 439 cm^{-1} is related to würtzite hexagonal phase characteristic of ZnO. Also this band was observed by Nehru (Nehru *et al*., 2012) and Yousefi (Yousefi *et al*., 2020) located at 439 cm^{-1} and 437 cm^{-1}, respectively. In the case of the Tb-doped ZnO (fig 2.b), the spectrum was complex and the values were slightly shifted (438, 518, 716 cm^{-1}) which may be perturbed by presence of Tb ions inside zinc oxide films. The peak at 716 cm^{-1} is generated by combinations of phononic and optical modes that describe longitudinal acoustic and transverse processes of the optical lattice. In irradiated samples, figs. 2c and 2d, Raman spectra were obtained such as a broad band centered about 1900 cm^{-1} for ZnO, and it was shifted to 2000 cm^{-1} for Tb-doped ZnO and less intensity was observed due to Tb ion impurity into host lattice. Photoluminescence (PL) spectra of ZnO and ZnO:Tb samples were made using an excitation line (λ_{exc}) of 350 nm. The PL spectra for the ZnO and ZnO:Tb samples were very different. In the undoped sample (fig. 3a) typical peaks of band-to-band transitions or near band edge (NBE) emissions (385 nm) were observed in the unirradiated sample.

Visible emissions in ZnO originated from oxygen vacancies to the valence band were exhibited such as bands centered approximately: 405, 426, and 450 nm. These bands were raised in their intensity when ZnO films were irradiated. The shoulder at 450 nm may be a phonon replica of the main peak located at 426 nm. (fig. 3b) (for unirradiated sample) exhibits a spectrum with visible ZnO emissions and typical emissions of Tb^{3+} ions superimposed. The unirradiated ZnO:Tb exhibited emissions at 490, 544, 582, and 620 nm due to the $^5D_4$-$^7F_{j=6,5,4,3}$ transitions of the Tb^{3+} ion in the ZnO phosphor. These values are in agreement with those emissions observed by radioluminescence (RL) on terbium-doped zinc oxide crystals by implanted Tb ions forming nanoparticles (Cetin *et al*., 2009). In the case of the irradiated samples (terbium-doped zinc oxide), inhibition of Tb emissions was detected, and appears a broad band (from 400 to 650 nm) centered at 502 nm. In several reports, this band is related to intrinsic defects, such as zinc and oxygen vacancies and interstitial oxygen (Isik *et al*., 2016; Cetin *et al*., 2009; Parta *et al*., 2013).

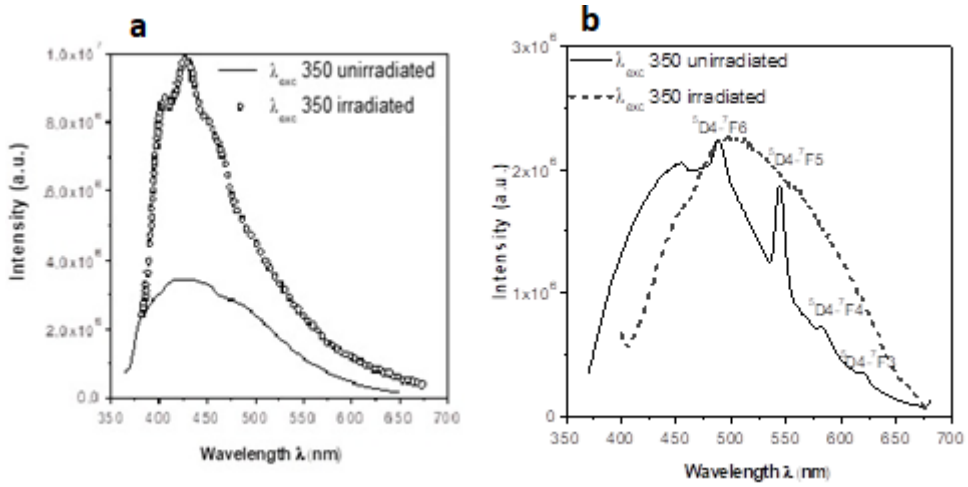

Fig. 3 Photoluminescence spectra of the samples, **a)** ZnO, and **b)** ZnO:Tb^{3+}. Unirradiated and gamma-irradiated samples.
Fig. 3. Espectros fotoluminiscentes de las muestras, **a)** ZnO y **b)** ZnO: Tb^{3+}. Muestras no irradiadas y e irradiadas con fotones gamma.

X-ray diffraction (XRD) measurements were carried out to investigate the crystalline structure of the ZnO and Tb-doped ZnO samples (figs. 4a and 4b), both patterns were identical. The diffractogram for ZnO:Tb (1 at.%) (fig. 4b) corresponds to the ZnO hexagonal wurtzite phase (JCPDS 36-1451) (Moura *et al*., 2010). It is possible to observe well-defined diffraction peaks and the highest intensity is obtained for $2\theta < 35°$, for (100) line, which could be associated with the preferred orientation along the c axis, as reported by Kumar (Kumar *et al*., 2013). Peaks for Tb compounds were not observed. This is indicative that the presence of the Tb ions in the ZnO host lattice does not disturb the crystalline structure. In this case, the doping concentration was about 1 at. %, probably the XRD technique may not be sensitive to these terbium quantities in this phosphor.

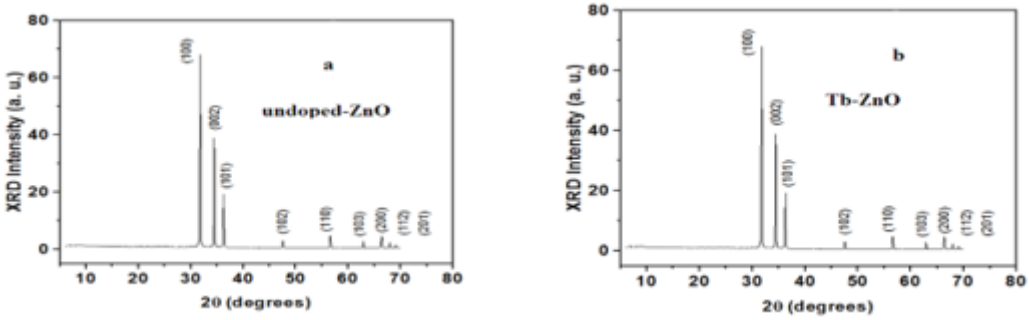

Fig. 4. XRD patterns of **a)** undoped ZnO, **b)**Tb-doped ZnO samples.
Fig. 4. Difractogramas de rayos X de **a**) muestra de ZnO no dopada, **b**)muestra de ZnO dopada con Tb.

Atomic effective number (Z_{eff})

The Z_{eff} was obtained due to the important characteristic of zinc oxide phosphor to expected for thermoluminescent (TL) response at different energies, in this case, exposed to gamma radiation. Considering that the material response depends on the atomic number *Z* of the constituents,

$$Z = \sqrt[x]{a_1 Z_1^x + a_2 Z_2^x + \ldots} \qquad (8)$$

$$\text{With } a_i = \frac{n_i(Z_i)}{\sum n_i(Z_i)} \text{ and } n_i = N_A Z_i$$

Where: a_1, a_2 … an are the fractional contents of electrons belonging to elements Z_1, $Z_2 \ldots Z_n$ respectively, n_i is the number of electrons belonging to each element Z_i and N_A is the Avogadro number. The value of x is 2.94 (Furetta, 2010). For undoped ZnO and Tb-doped ZnO preparations were obtained Ze_{ff} = 27.74 and Ze_{ff} = 56.47 values, respectively. Since the effective atomic numbers of the samples are about 4 and 8 times greater than that of human tissue (Ze_{ff} = 7.4) respectively, an accurate calibration should be done for its use in personal and high field radiation applications.

Thermoluminescence (TL) and computerized glow curve deconvolution (CGCD)

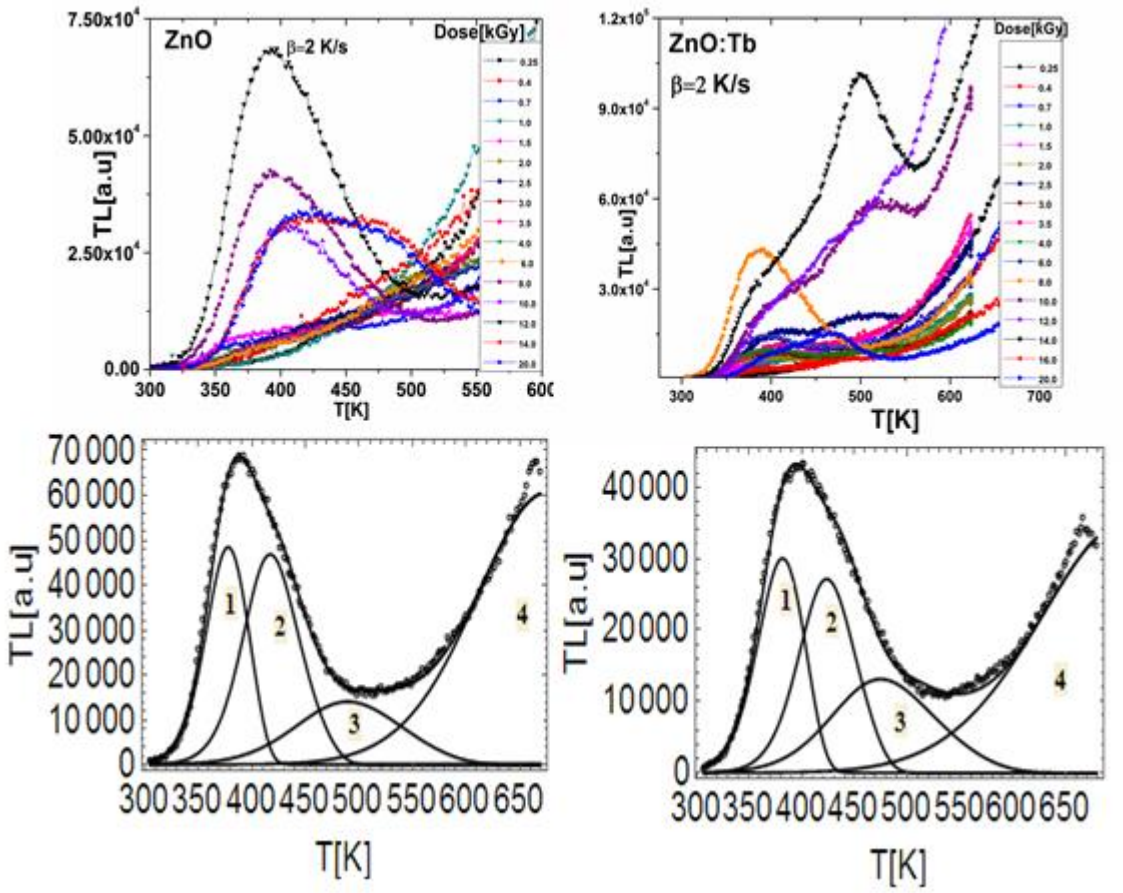

Fig. 5. a) and **b)** Glow curves as a function of doses: 0.25-20 kGy obtained with 2 K/s heating rate, **c)** and **d)** Deconvolution of the glow curves, assuming the mixed order kinetics model, the experimental glow curves (open circles) at the dose of 12 kGy and 170 Gy/min gamma dose rate, for undoped ZnO and Tb-doped ZnO, respectively.

Fig. 5. a) y **b)** Curvas de brillo como función de la dosis: 0.25-20 kGy obtenidas a una tasa de calentamiento de 2 K/s, **c)** y **d)** Deconvolución de las curvas de brillo asumiendo un modelo cinetico mixto, las curvas de brillo experimentales(círculos) obtenidas a una dosis de 12 kGy y a una tasa de dosis de 170 Gy/min, para las muestras de ZnO sin dopar y ZnO dopado con Tb, respectivamente.

The glow curves fig. 5a and 5b, exhibit a wide structure; in such case, a computerized glow curve deconvolution (CGCD) is useful to obtain kinetic parameters such as activation energy (E) and frequency factor (s); R_m and α parameters of the traps are involved in TL model too. The algorithm of deconvolution program is based on Mixed Order Kinetic model (Kitis *et al*., 2000; Chen *et al*., 1981; McKeever *et al*., 1985) given by the following expression:

$$I(T) = I_m \frac{\{exp((1-\Delta_m)/R_m)-\alpha\}^2}{exp((1-\Delta_m)/R_m)} \frac{exp\left\{\frac{E}{kT}\frac{T-T_m}{T_m}\right\} exp\left\{\frac{T^2}{T_m^2 R_m} exp\left(\frac{E}{kT}\frac{T-T_m}{T_m}\right)(1-\Delta_m)\right\}}{\left\{exp\left\{\frac{T^2}{T_m^2 R_m} exp\left(\frac{E}{kT}\frac{T-T_m}{T_m}\right)(1-\Delta)\right\}-\alpha\right\}^2} \qquad (9.a)$$

Where: k is Boltzmann constant, I_m and T_m are the maximum luminescence intensity and temperature in peak deconvoluted, respectively, and other quantities are: $\Delta = 2kT/E$, $\Delta_m = 2kT_m/E$, and $R_m = \frac{A_n}{A_m}$ where A_m is recombination probability and A_n is trapping probability, $\alpha = \frac{n_0}{n_0+c}$ is factor that directly determines the value of kinetic order in model of mixed-order kinetics and as a consequence α influences the shape of glow curve, c is a constant, and n_0 (cm^{-3}) is electron trap concentration. In R_m factor the explicit expression for A_m is:

$$A_m = Exp[\tfrac{A_m-\alpha}{A_m+\alpha}(1-\Delta_m)] \qquad (9.b)$$

The equation (9.b) is a definition of α, as an implicit function of two parameters α and Δ_m. The explicit form α cannot be obtained analytically but relationship of term A_m and parameter α was examined in a very broad region of parameters, α = 0.1-0.95, E = 0.6-2.2 eV, and s = 10^7-10^{22} s^{-1}. For this range of values, dependence of A_m on Δ_m can be neglected. So, R_m is obtained:

$$R_m = \frac{2.6-0.9203+0.324\alpha^{3.338}}{2.6-2.9203\alpha+0.324\alpha^{3.338}} \qquad (9.c)$$

And finally, frequency factor s is defined by:

$$s = \frac{\beta E}{k\,T_m^2} R_m \left(\frac{\alpha}{1-\alpha}\right) exp\left(\frac{E}{k\,T_m}\right) \qquad (9.d)$$

The curve fitting procedure was performed using the Figure of Merit (FOM). A FOM equal to or less than 5 % means an acceptable fit (Balian *et al*., 1977). In fig. 5c glow curve of sample A shows one wide resolved peak, at 450 K, as shown in fig. 5d, glow curve of sample B is quite similar to previous one: first peak appears at 475 K. The TL glow curves for both preparations were similar.

Table 1. Kinetic parameters as obtained by CGCD for A (ZnO), and B (ZnO:Tb) samples.
Tabla 1. Parámetros cinéticos obtenidos por deconvolución de las curvas de brillo para las muestras A(ZnO), y B(ZnO:Tb).

Peak number	T_m [K]	R_m	α	*E* [eV]	*s* [s^{-1}]	Peak area [counts]	Peak number	T_m [K]	R_m	α	*E* [eV]	*s* [s^{-1}]	Peak area [counts]
β= 2K/s	Sample A:ZnO, FOM=0.02						Sample B: ZnO: Tb, FOM= 0.03						
1	385	1.68	0.45	0.65	5.39E+07	2.43E+06	1	385	2.51	0.63	0.76	3.18E+09	1.67E+06
2	441	1.97	0.53	0.67	5.39E+07	3.16E+06	2	441	6.55	0.85	0.77	6.75E+08	1.83E+06
3	500	2.38	0.61	0.64	6.61E+05		3	500	2.93	0.68	0.5	1.95E+04	
4	655	1.08	0.1	0.51	52.7728		4	640	1.08	0.1	0.59	3.80E+02	

In almost all glow curve deconvolutions of samples (A and B), R_m values were greater than or equal to unity, therefore trapping process is predominant, as shown in table 1. Finally, the assumption of mixed order kinetics (MOK) comparing with other models, as general order kinetics (GOK), is more useful because MOK has a physical basis (Sadek *et al*., 2014). The greatest R_m values were for sample B (Tb-doped ZnO), hence Tb ions promote capture of charge carrier.

When the zinc oxide samples were prepared by the co-precipitation method (Parta *et al*., 2013) they were composed by nanorods which showed broad glow curves peaked at 530 K (255 °C) for Tb-doped ZnO and 465 K (190 °C) for undoped sample. The activation energy (*E*) and frequency factors (*s*) obtained by Chen´s method were 0.98 eV and 2.77×10^8 s^{-1}, respectively, for ZnO:Tb. Both peaks, 530 K and 465 K, follow the first-order kinetics and other satellite peaks at lower side temperature of glow curves obey second-order kinetics. Pal and co-workers (Pal *et al*., 2006) reported the TL of undoped ZnO spherical particles as nanophosphor obtained using glycol mediated chemical synthesis. Two glow peaks at 420 K (second-order) and 490 K (first-order) deconvolved by a computer fitting program, with activation energy about 0.8 eV and 1.2 eV, and frequency factor at 7×10^8 and 1×10^{12} s^{-1}, respectively, were obtained. It seems that TL glow curves are influenced by preparation methods and also by heating rate. However in this last case, if it is considered separately, each of four TL peaks (table 1) in which the whole glow curves of samples A and B are deconvolved shows a slight shift to higher temperatures as dose increases. But the overlap of peaks 1, 2, and 3 give rise to experimentally recorded high-temperature peak, the maximum of which does not shift as dose was increased. The results indicate a variation of activation energy *E* as a function of heating rate; this has been attributed to temperature lag and decrease of TL intensity as well as to activation energy and can be referred to as a thermal quenching effect(Gökce *et al*., 2009). However, if variation of *E* is due to temperature lag one should expect same variation for all peaks. Therefore, an analysis of

temperature lag in TL glow-curve measurement is necessary and its implementation is described in next section.

Temperature lag in TL glow curve measurement analysis

Due to variation in kinetic parameters and effects on structure of glow curves, a compute of theoretical model proposed by Kitis (Kitis *et al*., 1998) will be carried out to correct for temperature lag in TL glow curve. The relationship among α-values and kinetics order (b) showed that overall scattering of values obtained for b corresponding to any value found of α was within approximately ±10% (Sunta *et al*., 2002). The α-values for peaks 1, 2, and 3 of samples A, B were found to be 0.4–0.6 evidencing that b ranged between 1.2 and 1.4 values. Then use of model given by equation (10) to correct lag in TL glow-curve is adequate(Kitis et al., 1998), and T_j temperature is necessary to evaluate:

$$T_j = T_i - c\, Ln\left(\frac{\beta_i}{\beta_j}\right) \qquad (10)$$

Where $c = T_i T_j \frac{k}{E}$, k is Boltzmann constant, and taking the case that T_i and T_j are peak maximum temperatures T_m, obtained for two different rates of heating $\beta_i < \beta_j$, and $T_i < T_j$. The glow peak due to heating rate β_i is shifted towards higher temperatures, where: $\Delta T = T_g - T_m$, $T_g = T_0 + \beta t$, $T_m = T_0 + \beta_{eff}\, t$ and last term β_{eff} is obtained:

$$\beta_{eff} = \frac{T_g - T_0 - \Delta T}{T_g - T_0}\beta \qquad (11)$$

As activation energies of undoped ZnO deconvoluted glow peaks are too close; 0.65 eV, 0.67 eV, and 0.64 eV (table 1), only that of first peak deconvolved was computed to validate equation (10).

The results of the analysis for this approximation are shown in table 2. The theoretically evaluated glow peak maximum temperatures are listed in column 2 for E = 0.65 eV. Analogously, equation (10) was applied only to the first and third deconvoluted glow peaks of the Tb-doped ZnO sample (table 3).

Table 2. Results testing validity of equation (10) for peak 1 deconvolved (ZnO).
Tabla 2. Resultados probando la validez de la ecuación (10) en el pico deconvolucionado 1.

E=0.65 eV, s=5.39×10^{7}s^{-1}							
β[K/s]	T_m [K]	$T_i\,T_j$ [K^2] [×10^5]	c_1	$T_{m\,n}$ [K]	$\Delta T[K]$	T_g[K]	β_{eff}[K/s]
2	377.08	1.4219	1.0000	377.77	0.6931	385	1.87
5	393.39	1.4834	1.0433	394.12	0.7231	416	4.23
10	406.66	1.5334	1.0784	407.40	0.7475	404	10.26
15	415.6	1.5642	1.1001	415.6	0.7625	404	16.33
20	420.81	1.5868	1.1160	421.58	0.7735	454	16.42
40	435.92	1.6438	1.1561	436.72	0.8013	454	36.18

Table 3. Results testing validity of equation (10) for peaks 1 and 3 deconvolved (ZnO:Tb).
Tabla 3. Resultados probando la validez de la ecuación (10) en los picos deconvolucionados 1 y 3 (ZnO:Tb).

E=0.5 eV			s=1.95E+04[s^{-1}]				
β[K/s]	T_m[K]	T_iT_j[K^2]x10^5	c_1	T_{mn}[K]	ΔT[K]	T_g[K]	β_{eff}[K/s]
2	455.63	2.076	1	456.32	0.693	500	1.62
5	485.64	2.2127	1.066	486.38	0.739	500	4.70
10	510.9	2.3278	1.121	511.67	0.777	495	10.75
15	526.82	2.4003	1.156	527.62	0.802	500	16.83
20	538.69	2.4544	1.182	539.51	0.82	524	21.24
40	569.39	2.5943	1.25	570.26	0.866	530	46.27
E=0.77 eV			s=6.75E+08[s^{-1}]				
β[K/s]	T_m[K]	T_iT_j[K^2]x10^5	c_1	T_{mn}[K]	ΔT[K]	T_g[K]	β_{eff}[K/s]
2	397.77	1.5822	1	398.46	0.693	441	1.49
5	413.2	1.6436	1.039	413.92	0.72	470	3.58
10	425.65	1.6931	1.07	426.39	0.742	455	8.43
15	433.25	1.7234	1.089	434.01	0.755	475	11.96
20	438.83	1.7456	1.103	439.6	0.765	495	15.01
40	452.82	1.8012	1.138	453.61	0.789	470	36.67

Tables 2 and 3 show that approximation of equation (10) gives acceptable results for a quite large range of used heating rates (1-40 K/s) thus validating it for their use. Glow peak shifts for lower heating rates (2–5 K/s) are about 15 K, which is easily measured. Furthermore, the constant c_1 is very sensitive to T_m, which should be calculated within an accuracy better than 1 K. This is not difficult for low heating rates. The measurements at low rates of heating are the reference, so they need special attention to avoid temperature lags as a high-temperature gradient in sample (Kitis *et al*., 1998; Bos *et al*., 1992).

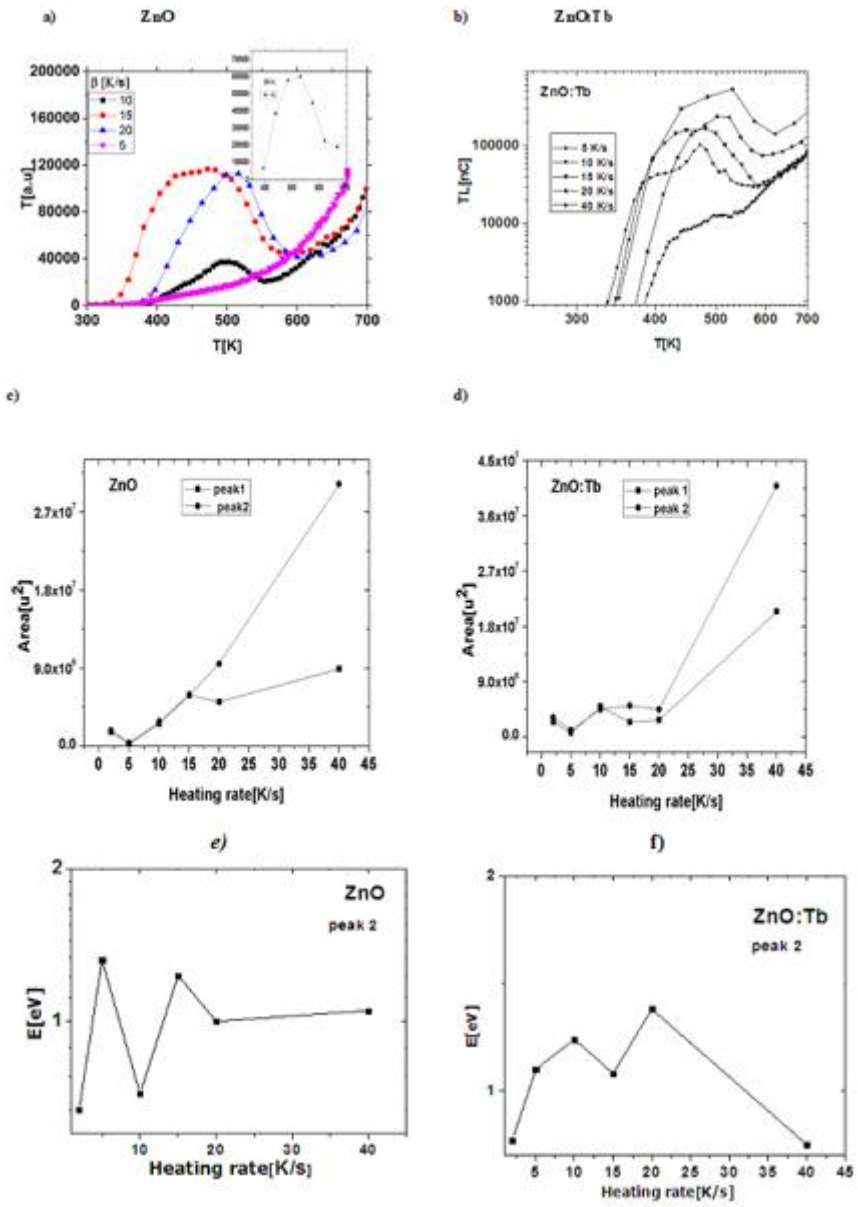

Fig. 6. a) and **b**) Glow curve as a function of the heating rate from 5 to 40 K/s, **c)** and **d**) integrated TL for peaks 1 and 2, and **e)** and **f**) activation energy (*E*) values as a function 2-40 K/s heating rate.
Fig. 6. a) y **b**) Curvas de brillo como función de la tasa de calentamiento de 5 a 40 K/s, **c)** y **d)** intensidad TL integrada para los picos de brillo 1 y 2, y **e)** y **f)** valores de energía de activación (*E*) como función de la tasa de calentamiento de 2-40 K/s.

As heating rate grows, it produces two pronounced effects on glow curves of zinc oxide: a TL emission increase and a considerable broadening of peak located at 420 K occur as shown in figs. 6a and 6b. Temperature lag at higher readout heating rates also influences determination of *E* values by glow curve fitting. As shown in figs. 6c and 6d, integrated TL intensities maximum and minimum occurred for 5 and 40 K s^{-1} for both samples, respectively. However, a more detailed explanation for variation of integrated TL intensity and peak intensity with heating rate may be achieved by considering influence of more than one effect involved in TL

of zinc oxide. Considering peak 2 (figs. 6e and 6f) for ZnO and ZnO:Tb, respectively, a variation of activation energy for different heating rate and a strong decay of *E* value at 40 K/s for ZnO:Tb were observed. It seems that Tb impurity in zinc oxide modifies TL mechanism and then behavior of activation energy. The Tb^{3+}-vacancy and clusters can be participating during heating rate, and also defect interaction with different time reactions for low and a high heating rate may occur increasing integrated area of glow curves (Piters *et al*., 1993; Subedi *et al*., 2010; Cuz-Zaragoza *et al*., 2011). It should be taken into account that temperature lags involved also a complex TL mechanism because recombination of several types of defects occurred during heating stimulation; the T_m, total area of glow curves, and activation energy (*E*) values can be affected by dopant cluster and thermal quenching. Almost two stages were observed for Tb-doped ZnO (fig. 6f); *E* increased from 2-10 K/s, and a variation from 15 K/s and decay at 40 K/s. This last decay may occur due to large reaction time at that high heating rate. If the variation of activation energy (*E*) is due to the temperature lag same evolution should be expected for all peaks of zinc oxide.

Annealing effect on the TL signals and signal reproducibility

The effect of thermal treatment as annealing is to stabilize trap levels so that in subsequent uses both intrinsic background and TL response should be reproducible. The zinc oxide samples were annealed in a tube furnace at 350 K for 60 min and then cooled down up to room temperature, after that all the samples were irradiated with 12 kGy of gamma photons from a ^{60}Co source irradiator.

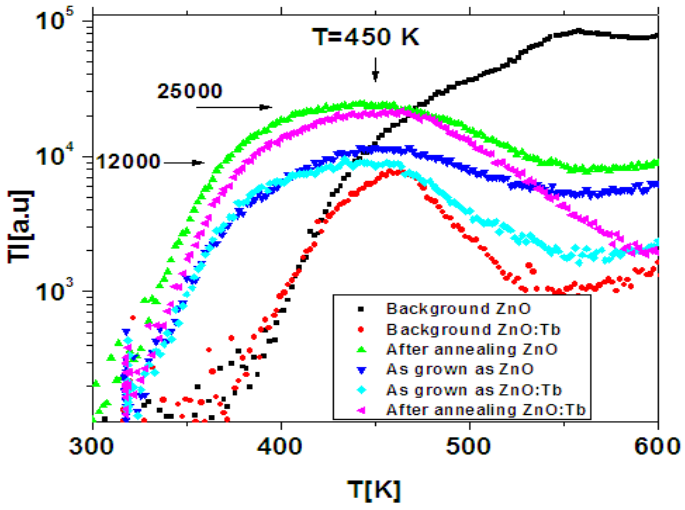

Fig. 7. Glow curves of undoped ZnO and Tb-doped ZnO phosphors with a dose of 12 kGy.
Fig. 7. Curvas de brillo de los fosforos ZnO sin dopar y de ZnO dopado con Tb a una dosis de 12 kGy.

The annealing effect on zinc oxide samples shows a complex structure of their glow curves (fig. 7) which peaked around 450 K. The TL intensity of ZnO: Tb was observed to be less than that of undoped ZnO. The TL signals of both samples grown by a factor of 2 after annealing. It implicates that a major quantity of defects as vacancies was generated in samples with previous annealing treatment. The TL signal of ZnO samples increases as annealing temperature enhanced, and does not alter the value of peak temperature and is the optimized temperature for heating samples (Raunak *et al*., 2015).

The reproducibility of TL signals as a function of readout cycles should be characterized for a phosphor with a dosimetric purpose. Furetta (Furetta, 2010) gives a procedure to check reproducibility of TL signal as a function of successive irradiation-readout cycles. The coefficient of variation (CV) for TL dosimeter is given by:

$$CV = \frac{\sigma}{m} \qquad (15)$$

Where: σ and m are standard deviation and average value of 10 repeated readings of dosimeter, respectively. The half-width of confidence interval μ is given by $\mu = CV\frac{t}{\sqrt{2(n-1)}}$ where n is number of repeated cycles and t is value of student test. In present case $n = 10$ and $t = 2.26$ at a confidence level of 95 %. Then $\mu = 0.53\,CV$ and reproducibility test for dosimeters is acceptable if $CV + \mu \leq 7.5\%$. Which transforms, considering last equation in following acceptable level $CV \leq 5\%$. So for data of successive irradiation-readout cycles, it was obtained: $m_A = 39.52, \sigma_A = 11.84, m_B = 57.87, \sigma_B = 32.56,$ and consequently the variability coefficient of TL reproducibility signal for samples ZnO and ZnO:Tb was ranging among 29 and 57 %, respectively. At this point, it is an important remark about improving reproducibility of TL signals if it is considered to erase first glow peak deconvolved at 385 K, due to its high instability under fading showed by Park et. al. in undoped ZnO (Park *et al*., 2014), while other peaks at a higher temperature (441 and 500 K) exhibited an acceptable TL reproducibility signal as reported by Pal and Manam for ZnO and ZnO:Tb (Pal *et al.*, 2013). Therefore, herein CV coefficient for undoped-ZnO and Tb-doped ZnO exhibit strong variations when whole glow curves were measured. Following, due to CV variation values, linearity analysis of dose-response was carried out for zinc oxide phosphor.

TL dose-response and linearity analysis

At 0.25 kGy gamma dose threshold was enough to generate main TL mechanism to detect TL signal, i.e., samples were sensible at that dose. The TL dose-response exhibited three stages (fig. 8a): at relatively low doses (stage 1, 0.25-4 kGy) there was unclear linearity, at intermediate doses (stage 2, 6-12 kGy) both samples ZnO and ZnO:Tb showed an almost linear response, and at higher doses (stage 3,14-20 kGy) TL response showed a slowly steep increase.

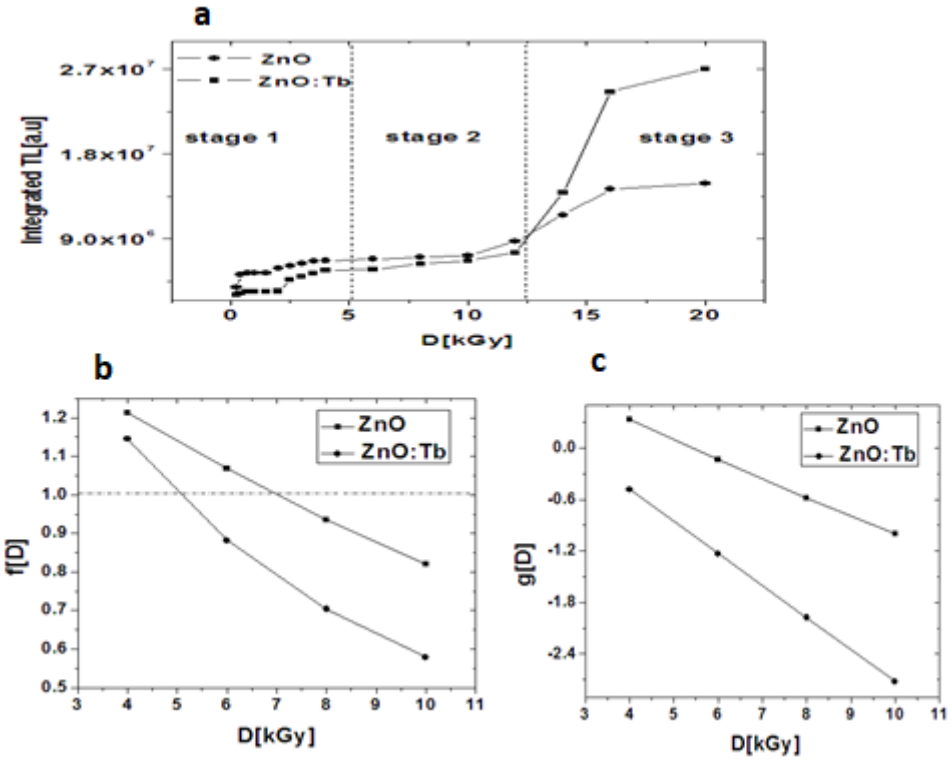

Fig. 8. a) Integrated TL dose-response of ZnO and Tb-doped ZnO, **b)** Supralinearity index, **c)** Superlinearity index.

Fig. 8. a) Respuesta TL-dosis integrada de ZnO sin dopar y ZnO, dopado con Tb, **b)** índice de supralinealidad, **c)** índice de superlinealidad.

The linearity at stage 2 range will be analyzed with more detail by supralinearity index f(D) and superlinearity index g(D), given by:

$$f(D) = \frac{M(D)/D}{M(D_L)/D_L} \qquad (12)$$

$$g(D) = \frac{D\,M''(D)}{M'(D)} + 1 \qquad (13)$$

With: $M(D) = M_1\left[1 - \exp\left(-\frac{D}{E01}\right)\right] + M_2\left[1 - \left(1 + \frac{D}{E02}\right)\exp\left(-\frac{D}{E02}\right)\right]$ (14)

Where: $M'(D)$, $M''(D)$ are the first and second derivative of $M(D)$, M_1, M_2 are TL contributions of each saturating exponential, and $E01$, $E02$ are the saturation doses of each contribution (Larson *et al.*,1976; Waligorsky *et al.*,1980; Waligorsky *et al.*,1993). These indexes characterize linearity of response, namely: $f(D) > 1$, $f(D) = 1$ or $f(D) < 1$ indicate supralinearity, linearity, or sublinearity, respectively, while $g(D) > 1$, $g(D) = 1$ or $g(D) < 1$ indicate superlinearity, linearity o sublinearity respectively. The supralinearity index *f(D)* (fig. 8b) shows a switch from a supralinear behavior for doses below 5.5 kGy, to a sublinear one for greater doses. The superlinear index $g[D]$ (fig. 8c), shows a negative value for whole range. Despite these materials does not show clear linearity under these conditions, they should not be rejected as a radiation detector for high doses (i.e. kGy), and should be improved maybe modifying preparation method using a different annealing process and a codoping impurity in zinc oxide phosphor.

Fading of the TL signals

TL fading signal as a function of elapsed time can be useful in routine TL measurement and allows to characterize the TL signals decay of phosphor exposed to a radiation field. Zinc oxide samples were gamma-irradiated and they were stored in a dark environment. The TL signal was readout periodically for ZnO and ZnO:Tb samples, respectively, during 42 days (fig. 9). Considering initial irradiation of samples followed by fading at room temperature and assuming first-order kinetics, for a storage time $t_s >> t_i$ (irradiation time), following expression simulated this case is (Kitis *et al.*, 2005; Gomez-Ros *et al.*, 1996): $\Phi = \Phi_0 \exp(-pt)$ and then $p = (-1/t)\ln(\Phi/\Phi_0)$, where Φ can be considered integrated glow curve or peak area. So by taking into account at final 42 days of fading; $p = 0.149$ d^{-1} or 14.9 % lost per day of TL signal for ZnO, and 15.9 % for ZnO:Tb. The constant *p* is less fast decay for undoped zinc oxide than that for Tb-doped ZnO.

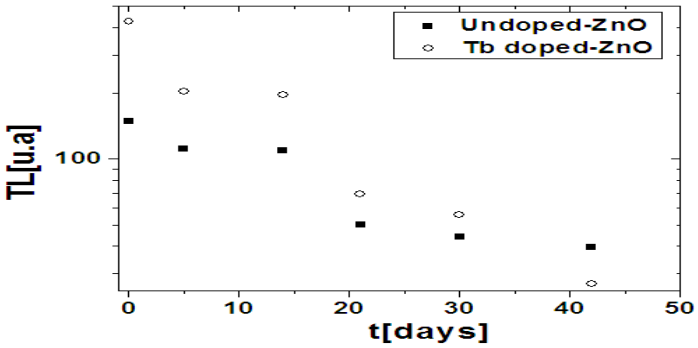

Fig. 9. TL-Fading of ZnO and ZnO:Tb phosphor.
Fig. 9. Desvanecimiento de la señal TL, para los fósforos ZnO y ZnO:Tb.

In this case, Tb ions in ZnO contribute to stabilizing intrinsic defects in zinc oxide and well defined glow curves as can be seen in fig. 7 too. It seems that fading observed in ZnO also depends on their preparation method and their thermal history.

Conclusion

Micro-nanostructured undoped ZnO and Tb-doped ZnO films obtained by Spray Pyrolysis method have been characterized using SEM, Raman, XRD, PL, and analyzed their TL characteristics. PL emission of unirradiated ZnO:Tb exhibited defined bands at 490, 544, 582, and 620 nm due to $^5D_4$-$^7F_{j=6,5,4,3}$ transitions belonging to Tb^{3+} ions. The presence of terbium ions in ZnO contributes to obtaining larger hexagonal rods (especially larger diameter ones) and increased TL response after annealing process. Results suggest that zinc oxide films are sensible to high dose (0.25 kGy) in a gamma field radiation. Four peaks were deconvolved by CGCD method assuming Mixed Order Kinetics model that well fitted glow curves. Variation of activation energy *E* as a function of heating rate has been attributed to temperature lag. The presence of Tb ions, in host material, improves TL response but also increases the coefficient of variation of TL signal. TL fading behavior was similar for ZnO and ZnO:Tb.

Acknowledgements

The authors are quite grateful to the National Polytechnic Institute (ESFM, CNMN, SIP and COFAA) and the National Autonomous University of Mexico (ICN and IIM). Finally, E. Cruz-Zaragoza acknowledges PAPIIT-DGAPA-UNAM Mexico through project number IG101119.

References

Ahsanulhaq, Q., Umar, A., & Hahn, Y. B. (2007). Growth of aligned ZnO nanorods and nanopencils on ZnO/Si in aqueous solution: growth mechanism and structural and optical properties. *Nanotechnology*, *18*(11), 115603. https://doi.org/10.1088/0957-4484/18/11/115603

Badalawa, W., Matsui, H., Osone, T., Hasuike, N., Harima, H., & Tabata, H. (2011). Correlation between structural and luminescent properties of Eu 3+ -doped ZnO epitaxial layers. *Journal of Applied Physics*, *109*(5), 053502. https://doi.org/10.1063/1.3549633

Balian, H. G., & Eddy, N. W. (1977). Figure-of-merit (FOM), an improved criterion over the normalized chi-squared test for assessing goodness-of-fit of gamma-ray spectral peaks. *Nuclear Instruments and Methods*, *145*(2), 389–395. https://doi.org/10.1016/0029-554X(77)90437-2

Baruah, S., & Dutta, J. (2009). Hydrothermal growth of ZnO nanostructures. *Science and Technology of Advanced Materials*, *10*(1), 013001. https://doi.org/10.1088/1468-6996/10/1/013001

Bos, A. J. J., Vijverberg, R. N. M., Piters, T. M., & McKeeve, S. W. S. (1992). Effects of cooling and heating rate on trapping parameters in LiF:Mg, Ti crystals. *Journal of Physics D: Applied Physics*, *25*(8), 1249–1257. https://doi.org/10.1088/0022-3727/25/8/016

Bos, A. J. J. (2001). High sensitivity thermoluminescence dosimetry. *Nuclear Instruments and Methods in Physics Research Section B: Beam Interactions with Materials and Atoms*, *184*(1–2), 3–28. https://doi.org/10.1016/S0168-583X(01)00717-0

Cetin, A., Kibar, R., Selvi, S., Townsend, P. D., & Can, N. (2009). Luminescence properties of Tb implanted ZnO. *Physica B: Condensed Matter*, *404*(20), 3379–3385. https://doi.org/10.1016/j.physb.2009.05.019

Chen, R., & Kirsh, Y. (1981). Analysis of Thermally Stimulated Processes. In *Pergamon Press*. ISBN: 9781483285511.

Cruz-Vázquez, C., Orante-Barrón, V. R., Grijalva-Monteverde, H., Castaño, V. M., & Bernal, R. (2007). Thermally stimulated luminescence of new ZnO–CdSO4 exposed to beta radiation. *Materials Letters*, *61*(4–5), 1097–1100. https://doi.org/10.1016/j.matlet.2006.06.055

Cruz-Zaragoza, E., González, P. R., Azorín, J., & Furetta, C. (2011). Heating rate effect on thermoluminescence glow curves of LiF:Mg,Cu,P+PTFE phosphor. *Applied Radiation and Isotopes*, *69*(10), 1369–1373. https://doi.org/10.1016/j.apradiso.2011.05.033

Daksh, D., & Agrawal, Y. K. (2016). Rare Earth-Doped Zinc Oxide Nanostructures: A Review. *Reviews in Nanoscience and Nanotechnology*, *5*(1), 1–27. https://doi.org/10.1166/rnn.2016.1071

Furetta, C. (2009). *Handbook of Thermoluminescence*. WORLD SCIENTIFIC. https://doi.org/10.1142/7187

Gökçe, M., Oğuz, K. F., Karalı, T., & Prokic, M. (2009). Influence of heating rate on thermoluminescence of Mg 2 SiO 4 : Tb dosimeter. *Journal of Physics D: Applied Physics*, *42*(10), 105412. https://doi.org/10.1088/0022-3727/42/10/105412

Gomez Ros, J. ., Delgado, A., Furetta, C., & Scacco, A. (1996). *Effects of simultaneous release of trapped carriers and pair production on fading in thermoluminescent materials during storage in radiation fields*. *Radiat Meas.* 26(2), 243-251. https://doi.org/10.1016/1350-4487(95)00301-0

Goswami, L., Aggarwal, N., Singh, M., Verma, R., Vashishtha, P., Jain, S. K., Tawale, J., Pandey, R., & Gupta, G. (2020). GaN Nanotowers Grown on Si (111) and Functionalized with Au Nanoparticles and ZnO Nanorods for Highly Responsive UV Photodetectors. *ACS Applied Nano Materials*, *3*(8), 8104–8116. https://doi.org/10.1021/acsanm.0c01539

Isik, M., Yildirim, T., & Gasanly, N. M. (2016). Thermoluminescence properties of ZnO nanoparticles in the temperature range 10–300 K. *Journal of Sol-Gel Science and Technology*, *78*(1), 76–81. https://doi.org/10.1007/s10971-015-3919-6

Katz, R. (1993). A track physics retrospective. *Radiat. Prot. Dosimetry* 47, 65-68.https://doi.org/10.1093/oxfordjournals.rpd.a081703

Kitis, G., & Furetta, C. (2005). Simulation of competing irradiation and fading effects in thermoluminescence dosimetry. *Radiation Effects and Defects in Solids*, *160*(7), 285–296. https://doi.org/10.1080/10420150500331438

Kitis, G., & Gomez-Ros, J. M. (2000). Thermoluminescence glow-curve deconvolution functions for mixed order of kinetics and continuous trap distribution. *Nuclear Instruments and Methods in Physics Research Section A: Accelerators, Spectrometers, Detectors and Associated Equipment*, *440*(1), 224–231. https://doi.org/10.1016/S0168-9002(99)00876-1

Kitis, G., & Tuyn, J. W. N. (1998). A simple method to correct for the temperature lag in TL glow-curve measurements. *Journal of Physics D: Applied Physics*, *31*(16), 2065–2073. https://doi.org/10.1088/0022-3727/31/16/017

Klingshirn, C. (2007). ZnO: Material, Physics and Applications. *ChemPhysChem*, *8*(6), 782–803. https://doi.org/10.1002/cphc.200700002

Kucuk, N., Kucuk, I., Yüksel, M., & Topaksu, M. (2016). Thermoluminescence characteristics of Zn(BO 2) 2 :Ce 3+ under beta irradiation. *Radiation Protection Dosimetry*, *168*(4), 450–458. https://doi.org/10.1093/rpd/ncv360

Kumar, V., Singh, N., Mehra, R. M., Kapoor, A., Purohit, L. P., & Swart, H. C. (2013). Role of film thickness on the properties of ZnO thin films grown by sol-gel method. *Thin Solid Films*, *539*, 161–165. https://doi.org/10.1016/j.tsf.2013.05.088

Larsson, L., & Katz, R. (1976). Supralinearity of thermoluminescent dosimeters. *Nuclear Instruments and Methods*, *138*(4), 631–636. https://doi.org/10.1016/0029-554X(76)90009-4

McKeever, S. W. S. (1985). *Thermoluminescence of Solids*. Cambridge University Press. https://doi.org/10.1017/CBO9780511564994

de Moura, A. P., Lima, R. C., Moreira, M. L., Volanti, D. P., Espinosa, J. W. M., Orlandi, M. O., Pizani, P. S., Varela, J. A., & Longo, E. (2010). ZnO architectures synthesized by a microwave-assisted hydrothermal method and their photoluminescence properties. *Solid State Ionics*, *181*(15–16), 775–780. https://doi.org/10.1016/j.ssi.2010.03.013

Nehru, L. C., Swaminathan, V., & Sanjeeviraja, C. (2012). Rapid synthesis of nanocrystalline ZnO by a microwave-assisted combustion method. *Powder Technology*, *226*, 29–33. https://doi.org/10.1016/j.powtec.2012.03.042

Özgür, Ü., Alivov, Y. I., Liu, C., Teke, A., Reshchikov, M. A., Doğan, S., Avrutin, V., Cho, S.-J., & Morkoç, H. (2005). A comprehensive review of ZnO materials and devices. *Journal of Applied Physics*, *98*(4), 041301. https://doi.org/10.1063/1.1992666

U., Meléndrez, R., Chernov, V., & Barboza-Flores, M. (2006). Thermoluminescence properties of ZnO and ZnO:Yb nanophosphors. *App Phys*, *89*, 177–183. https://doi.org/10.4028/0-00000-029-9

Pal, P. P., & Manam, J. (2013). Photoluminescence and thermoluminescence studies of Tb3+ doped ZnO nanorods. *Materials Science and Engineering: B*, *178*(7), 400–408. https://doi.org/10.1016/j.mseb.2013.01.006

Park, S. ., Hong, S., & Chae, Y. G. (2014). Thermoluminescence Fading in ZnO Irradiated by Beta-rays. New Physics. *Sae Mulli*, *6*, 580–585. https://doi.org/10.3938/NPSM.64580.

Piters, T., & Bos, A. J. J. (1993). A model for the influence of defect interactions during heating on thermoluminescence in LiF:Mg,Ti (TLD-100). *Appl Phys*, *26*, 2255–2265. http://dx.doi.org/10.1088/0022-3727/26/12/025

Rajendraprasad, M., Spriya, V., Sugiyama, M., & Ramakrishna, R. K. . (2013). Investigations on ZnO:Ni Layers Deposited by Spray Pyrolysis. *Hindawi Publishing Corporation*, 1–5. http://dx.doi.org/10.1155/2013/508170

Radovanovic, P. V., Norberg, N. S., McNally, K. E., & Gamelin, D. R. (2002). Colloidal Transition-Metal-Doped ZnO Quantum Dots. *Journal of the American Chemical Society*, *124*(51), 15192–15193. https://doi.org/10.1021/ja028416v

Raunak Kumar Tamrakar, Neha Tiwari, R.K. Kuraria, D.P. Bisen, Vikas Dubey, Kanchan Upadhyay. *Journal of Radiation Research and Applied Sciences* 2015 8 1-10. https://doi.org/10.1016/j.jrras.2014.10.005

Sadek, A. M., Eissa, H. M., Basha, A. M., & Kitis, G. (2014). Resolving the limitation of the peak fitting and peak shape methods in the determination of the activation energy of thermoluminescence glow peaks. *Journal of Luminescence*, *146*, 418–423. https://doi.org/10.1016/j.jlumin.2013.10.031

Sreedharan, R. S., Krishnan, R. R., Bose, R. J., Kavitha, V. S., Suresh, S., Vinodkumar, R., Sudheer, S. K., & Pillai, V. P. M. (2017). Visible luminescence from highly textured Tb 3+ doped RF sputtered zinc oxide films. *Journal of Luminescence*, *184*, 273–286. https://doi.org/10.1016/j.jlumin.2016.12.032

Shukla, S., Agorku, E., Mittal, H., & Mishra, A. (2014). Synthesis, characterization and photoluminescence properties of Ce3+-doped ZnO-nanophosphors. *Chemical Papers*, *68*(2). https://doi.org/10.2478/s11696-013-0442-5

Sunta, C. ., Ayta, W. E. ., Chubaci, J. F. ., & Watanabe, S. (2002). General order and mixed order fits of thermoluminescence glow curves—a comparison. *Radiation Measurements*, *35*(1), 47–57. https://doi.org/10.1016/S1350-4487(01)00257-8

Tamrakar, R. K., Tiwari, N., Kuraria, R. K., Bisen, D. P., Dubey, V., & Upadhyay, K. (2015). Effect of annealing temperature on thermoluminescence glow curve for UV and gamma ray induced ZrO2:Ti phosphor. *Journal of Radiation Research and Applied Sciences*, *8*(1), 1–10. https://doi.org/10.1016/j.jrras.2014.10.005

Umar, A., Karunagaran, B., Suh, E.-K., & Hahn, Y. B. (2006). Structural and optical properties of single-crystalline ZnO nanorods grown on silicon by thermal evaporation. *Nanotechnology*, *17*(16), 4072–4077. https://doi.org/10.1088/0957-4484/17/16/013

Waligórski, M. P. R., & Katz, R. (1980). Supralinearity of peak 5 and peak 6 in TLD-700. *Nuclear Instruments and Methods*, *175*(1), 48–50. https://doi.org/10.1016/0029-554X(80)90249-9

Yousefi, R., Jamali-Sheini, F., & Zak, A. K. (2012). A Comparative Study of the Properties of ZnO Nano/Microstructures Grown using Two Types of Thermal Evaporation Set-Up Conditions. *Chemical Vapor Deposition*, *18*(7–9), 215–220. https://doi.org/10.1002/cvde.201206979

Zhao, S., Wang, L., Yang, L., & Wang, Z. (2010). Synthesis and luminescence properties of ZnO:Tb3+ nanotube arrays via electrodeposited method. *Physica B: Condensed Matter*, *405*(15), 3200–3204. https://doi.org/10.1016/j.physb.2010.04.049